Journal of Vacuum Science & Technology A

Transport and Trap States in Proton Irradiated ultra-thick κ-Ga_2O_3

Running title: a concise title Proton Irradiated ultra-thick κ-Ga_2O_3

Running Authors: Polyakov et al.

A.Y. Polyakov[1], V.I. Nikolaev[1, 2], A.I. Pechnikov[1, 2], E.B. Yakimov[1,3], P.B. Lagov [1,4], I.V. Shchemerov[1], A.A. Vasilev[1], A.I. Kochkova[1], A.V. Chernykh[1], In-Hwan Lee[5], S.J. Pearton[6,a)]

[1]National University of Science and Technology MISiS, Moscow, Leninsky pr. 4, Moscow 119049, Russia
[2] Perfect Crystals LLC, 38k1 Toreza Avenue, off. 213, Saint Petersburg, 194223, Russia
[3]Institute of Microelectronics Technology and High Purity Materials, Russian Academy of Sciences, 6 Academician Ossipyan str., Chernogolovka, Moscow Region 142432, Russia
[4]Laboratory of Radiation Technologies, A. N. Frumkin Institute of Physical Chemistry and Electrochemistry Russian Academy of Sciences (IPCE RAS), Moscow 119071, Russia
[5]Department of Materials Science and Engineering, Korea University, Anamro 145, Seoul 02841, Republic of Korea
[6]Department of Materials Science and Engineering, University of Florida, Gainesville, FL 32611

[a)] Electronic mail: spear@mse.ufl.edu

Changes induced by irradiation with 1.1 MeV protons in the transport properties and deep trap spectra of thick (>80 μm) undoped κ-Ga_2O_3 layers grown on sapphire are reported. Prior to irradiation, the films had a donor concentration of ~10^{15} cm^{-3}, with the two dominant donors having ionization energies of 0.25 eV and 0.15 eV, respectively. The main electron traps were located at E_c-0.7 eV. Deep acceptor spectra measured by capacitance-voltage profiling under illumination showed optical ionization thresholds near 2 eV, 2.8 eV and 3.4 eV. The diffusion length of non-equilibrium charge carriers for ε-Ga_2O_3 was 70±5 nm prior to irradiation. After irradiation with 1.1 MeV protons to a fluence of 10^{14} cm^{-2} there was total depletion of mobile charge carriers in the top 4.5 μm of the film, close to the estimated proton range. The carrier removal rate was 10-20 cm^{-1}, a factor of 5-10 lower than in β-Ga_2O_3, while the concentration of deep acceptors in the lower half of the bandgap and the diffusion length showed no significant change.

I. INTRODUCTION

β-Ga_2O_3 is currently under intense study due to the large bandgap ~5 eV, electric breakdown field of~ 8 MV/cm, and electron saturation velocity of ~2000 cm/s which are favorable for applications in ultra-high-power electronic devices and solar blind photodetectors for the far-UV spectral range [1-8]. While the main interest has been in the thermodynamically stable monoclinic β-Ga_2O_3 polymorph, there is also great interest in metastable orthorhombic κ-Ga_2O_3 because of its high spontaneous electric polarization, which exceeds that of III-Nitrides [9,10]. This allows in principle to use that material for building heterojunctions with high density two-dimensional electron gases (2DEG) for high-power Field Effect Transistors (FETs) [11]. Such films are also often called ε-Ga_2O_3 based on initial attribution of their crystal symmetry to hexagonal type [10], the misapprehension cleared up by Cora et al. [12]. Although metastable, epitaxial films of κ-Ga_2O_3 polymorph can be grown on sapphire, there have also been demonstrations of growth on GaN, AlN or SiC by Halide Vapor Phase Epitaxy (HVPE) [13,14] and other epitaxial growth techniques, including Molecular Beam Epitaxy (MBE) [15] , Pulsed Laser Deposition (PLD) [16,17] or Mist Chemical Vapor Deposition (mist CVD)[18] . These films are stable up to temperatures about 800ºC or even higher if special measures are taken to protect the surface. Such increases of thermal stability have been reported for another metastable polymorph, corundum α-Ga_2O_3 whose thermal stability is even lower than for κ-Ga_2O_3 but can be increased from 600-700ºC to 900ºC using a cap layer of α-Al_2O_3 [19].

Heterojunctions of κ-Ga_2O_3 with wider-bandgap κ-$(Al_xGa_{1-x})_2O_3$ solid solutions [17] and multi-quantum-well (MQW) κ-$(Al_xGa_{1-x})_2O_3$/κ-Ga_2O_3 structures with varied Al mole fraction and hence the bandgap have been demonstrated for optimized

growth conditions [19]. The existence of 2DEG and Two-Dimensional Hole Gas (2DHG) at interfaces of heterojunctions formed by combining κ-Ga_2O_3 with different polar and nonpolar materials, such as polar basal plane GaN and AlN or nonpolar m-plane AlN have been theoretically predicted [20-23]. We have recently reported experimental observation of 2DHG at the κ-Ga_2O_3/AlN heterojunction [23]. The system is suitable for heterojunction engineering of multiple types of semiconductor devices. However, the tendency of κ-Ga_2O_3 films to grow in rotational microdomains with a high density of grain boundaries causing barriers for current flow between the grains and handicapping the in-plane conductivity, hampers the ability to fabricate useful devices [11,16]. Recently, several approaches to mitigate these structural problems have been described. One approach is Epitaxial Lateral Overgrowth (ELOG) in HVPE of κ-Ga_2O_3 on basal plane sapphire masked with patterns of SiO_2, which under optimized produced single-domain films with improved crystalline quality [24]. Growth of single domain κ-Ga_2O_3 has been demonstrated for mist CVD on ε/κ-$GaFeO_3$ substrates [25]. The crystalline quality of κ-Ga_2O_3 films prepared by HVPE on GaN/sapphire templates strongly improves for thicknesses >5-10 μm, [26,27] although it is not possible to fully suppress the rotational domains formation and the build-up of strain in the layers. The latter leads to separation of the growing layers from the substrates for thicknesses >20-30 μm. Growth of thicker films up to 86 μm was achieved if the films were deposited in several consecutive long runs. These films no longer showed features due to the presence of rotational domains, although the overall half-width of the symmetric and skew-symmetric x-ray reflections increased compared to 20-μm-thick layers [27]. Both 20-μm and 86-μm thick films showed, even when nominally undoped, large in-plane electric conductivity, low leakage

current of Schottky diodes, with donor concentrations of ~10^{15} cm^{-3}. The films also had a low density of deep traps and high photocurrent [26,27].

One aspect of κ-Ga_2O_3 that remains unexplored is the effect of non-ionizing energy loss from particle irradiation. This is relevant since one application for Ga_2O_3 is expected to be in extreme environments and the changes due to proton irradiation is a common approach to assess radiation hardness. In this paper, we report the first study of the effects of proton irradiation on transport properties and deep trap spectra of κ-Ga_2O_3.

II. EXPERIMENTAL

The layers used were grown in a similar fashion to earlier reports [27]. In brief, 86 μm thick κ-Ga_2O_3 was grown by HVPE on 4-μm-thick unintentionally doped (0001) GaN/sapphire template at 570°C at VI/III mole flow rate of 3, and growth rate 3 μm/h in 5 consecutive separate runs. The FWHM of the final product was 60 arcmin for the (004) symmetric reflection and the same for the (206) skew-symmetric reflection. For electrical and deep trap spectra characterization, circular Ni Schottky contacts with thickness 20 nm and diameter 1 mm and Ohmic contacts stripes of Au/Ti (80 nm/20 nm) were deposited using e-beam evaporation through a shadow mask. Characterization involved current-voltage (I-V) measurements with and without illumination, current-temperature (I-T), capacitance-frequency (C-f), capacitance-voltage(C-V), Admittance Spectra (AS) [28] and Deep Level Transient Spectroscopy (DLTS) [28]. I-V, C-V, C-f measurements were performed in the dark and under illumination with a set of Light Emitting Diodes (LEDs) with peak wavelength from 940- 277 nm and the wavelength half-width of 10 nm, while capacitance and AC conductance measurements were done for frequencies

between 20 Hz and 20 MHz in the temperature range 77-500K. In addition, the samples were imaged in the secondary electrons (SE), Microcathodoluminescence (MCL), and Electron Beam Induced Current (EBIC) modes of a Scanning Electron Microscope (SEM). The diffusion lengths of the non-equilibrium charge carriers L_d were obtained from fitting the dependence of the $I_c/(E_b \times I_b)$ on the probing SEM beam energy Eb [29], where I_c is the EBIC current, I_b is the probing beam of SEM current. These measurements were performed before and after irradiation with protons with fluence of 10^{14} cm^{-2} at 1.1 MeV, with a flux of 10^{11} cm^{-2}/s [30,31].

III. RESULTS AND DISCUSSION

I-V characteristics measured at room temperature in the dark and under illumination with the LED with peak photon energy 4.5 eV (peak wavelength 277 nm) are compared before and after proton irradiation in Fig. 1(a). The dark current is decreased by 40x at -1V after irradiation, while the photocurrent is decreased by 10x. The ideality factor for the forward branch increased from 1.7 to 2.4, the series resistance at room temperature increased from 10^6 Ω to 3.3×10^6 Ω, and the temperature dependence of the dark current at +2V showed an activation energy of 0.25 eV before irradiation and 0.15 eV after irradiation (see Fig. S1(a) in the Supplementary Material). The spectral dependence of photocurrent normalized by the dark current was similar in both cases (Fig. 1(b)) and showed optical thresholds near (1.3-1.5) eV, 2.3 eV, and 3.4 eV. The photocurrent normalized by dark current was much higher after irradiation, even though the absolute value of photocurrent was lower, which is explained by the even stronger decrease of the dark current. One can clearly observe the presence of three photocurrent increase

threshold energies near 1 eV, 2.3 eV, 3.5 eV in both spectral dependences. Those are likely related to the optical ionization cross sections of respective traps. It can also be seen that the photocurrent for above-bandgap excitation is an order of magnitude higher than for below-bandgap excitation before irradiation. This is no longer the case after irradiation because of the increased depth of the highly resistive region in the space charge of the Schottky diode of irradiated sample.

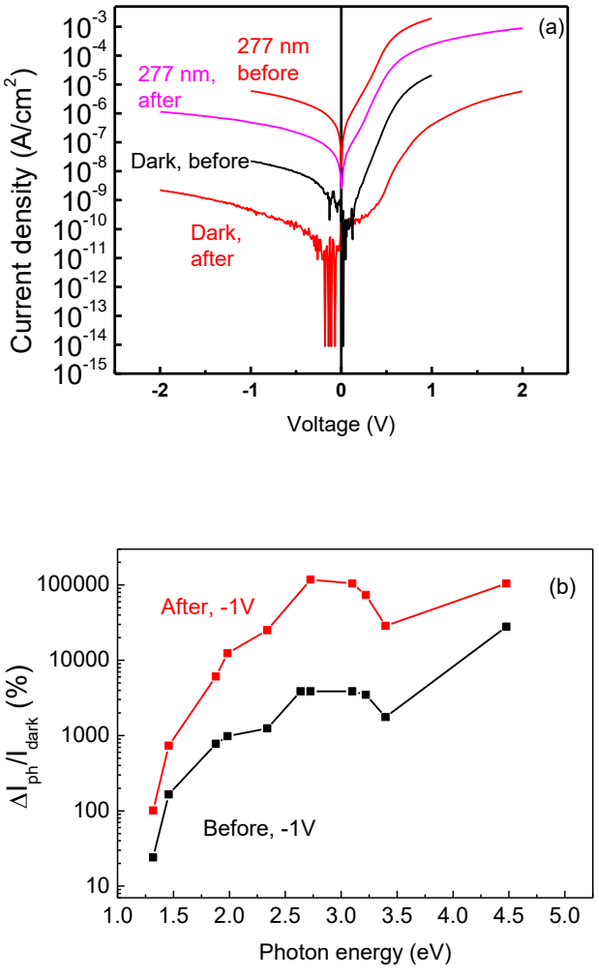

Fig. 1(Color online) (a) Room temperature I-V characteristics in the dark before (black line) and after (red line) irradiation with 1.1 MeV 10^{14} cm^{-2} protons; also shown are the I-

V characteristics before (red line) and after (magenta line) irradiation; (b) the spectra of photocurrent at -1V before and after irradiation.

The C-f characteristic at room temperature displayed a prominent step at frequencies below ~10 kHz and an approximate plateau at higher frequencies before irradiation (Fig. 2). After irradiation, the amplitude of the low frequency step was strongly diminished. Admittance spectra measurements indicated the presence of centers with activation energy of 0.25 eV at frequencies below 1 kHz, and 0.15 eV for frequencies above 1 kHz. At temperatures of~400K the derivative dC/dT showed peaks at frequencies below 0.1 kHz, indicating the presence of centers with activation energy 0.7 eV (See supplementary material at [URL will be inserted by AIP Publishing] for additional data on these properties, i.e. Fig. S2-S7 of the Supplementary Material). After irradiation, AS spectra showed the presence of centers with ionization energy of 0.15 eV (Fig. S2, S3 of the Supplementary Material). No signal from the 0.25 eV traps was detected.

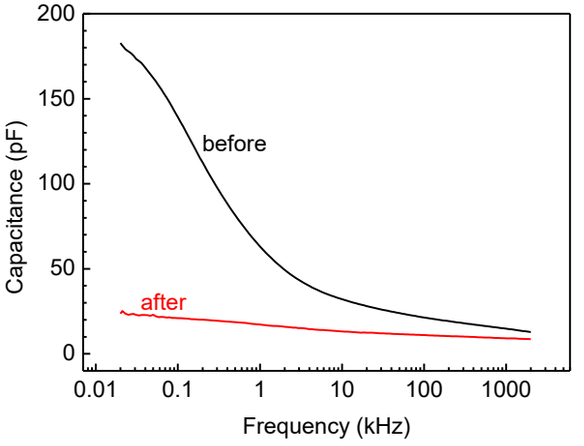

Fig. 2 (Color online) C-f characteristics measured at room temperature and 0V bias before (black line) and after (red line) irradiation.

C-V profiling at 90 Hz showed a carrier concentration of 2×10^{15} cm^{-3} at a depth of ~0.5 μm, which rapidly decreased at greater depths. Shallower donors with activation energy 0.15 eV in admittance were dominant for higher probing frequencies and could be seen for depths >2.5 μm (Fig. 3(a)). The concentration measured at low frequency is the sum of concentrations of the 0.25 eV and 0.15 eV donors. At high frequency, only the 0.15 eV donors are probed. The low frequency concentration dropped to approximately the concentration of the 0.15 eV donors at ~2 μm. If one assumes the concentration of the 0.15 eV donors near the surface is close to their concentration at 2.5 μm from the surface, then the surface density of 0.25 eV donors of 10^{15} cm^{-3} falls to zero below 2.5 μm. After irradiation, the 0.15 eV centers were predominant in admittance spectra (Fig. S2 of the Supplementary Material). C-V profiling of irradiated sample performed at 10 kHz yielded the profile of these donors shown in Fig. 3(a).

C-V measurements at 10 kHz performed under monochromatic illumination (LCV) [32] gave the photoinduced concentration spectra before and after irradiation presented in Fig. 3(b) (the raw $1/C^2$ versus voltage characteristics measured in the dark and under illumination with several photon wavelengths before irradiation are presented in Fig. S4 of the Supplementary Material;the actual LCV profiling results obtained by differentiating such $1/C^2$ versus V dependencies by voltage in the usual fashion are presented in Fig. S5, S6 of the Supplementary Material for the sample before and after irradiation). Before irradiation, the concentration of photoinduced carriers showed optical thresholds near 2 eV, 2.8 and 3.4 eV, with the latter two being predominant. The overall concentration of deep acceptors was ~10^{16} cm^{-3}. After irradiation, the 2eV optical

threshold was no longer observed, while the concentrations of deep acceptors with optical ionization thresholds near 2.8 eV and 3.4 eV are lower than before irradiation (Fig. 3(b)).

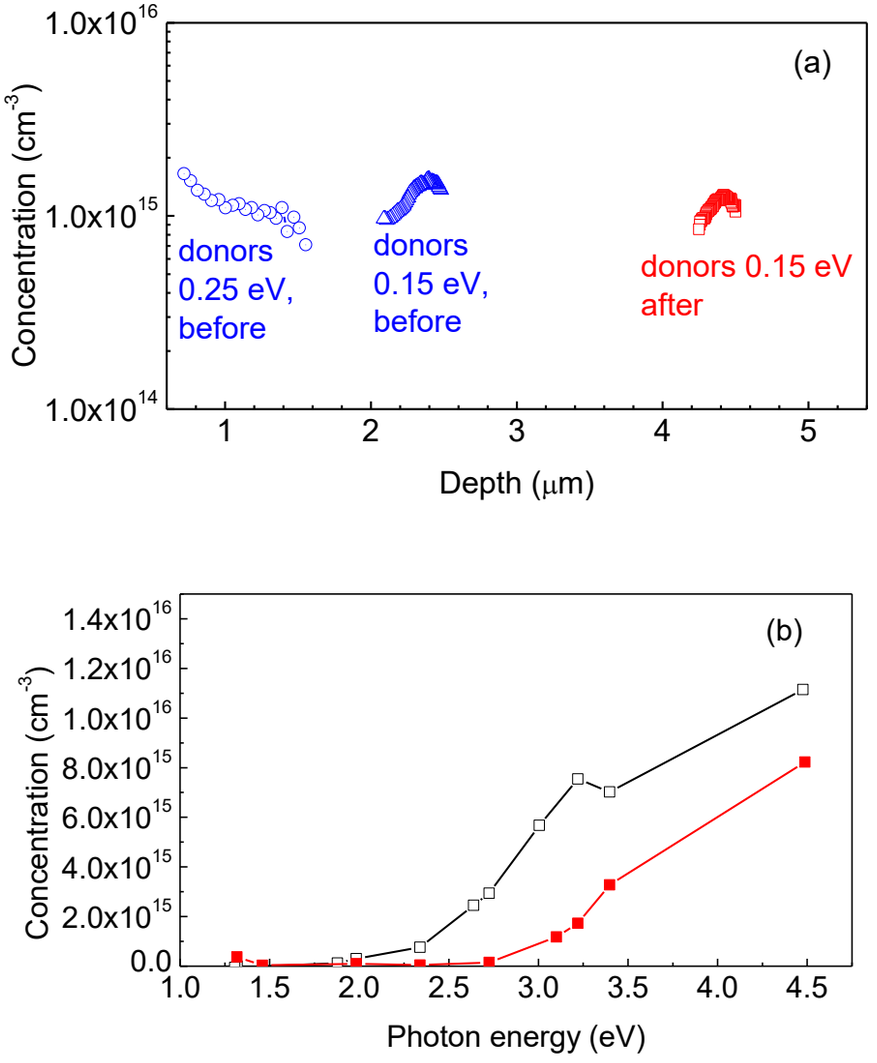

Fig. 3 (Color online) (a) profiles of 0.25 eV donors calculated from C-V measurements at 90 Hz (blue open circles), of 0.15 eV donors calculated from C-V measurements at 10 kHz (blue open triangles) for the sample before irradiation, and of 0.15 eV donors (red open squares) after irradiation; (b) concentrations of photoinduced electrons calculated from C-V profiling at 10 kHz before irradiation (open black squares) and after irradiation (solid red squares).

Deep electron traps spectra measured at 10 kHz, reverse bias -1V and forward bias pulse of +1V (50 ms long) are shown before and after irradiation in Fig. 4. Before irradiation, the spectra were dominated by deep traps at E_c-0.7 eV (electron capture cross section 7.8×10^{-15} cm^2). While it is difficult to accurately estimate the absolute concentration of the trap given the nonuniform distribution of donors with depth, if one assumes the space charge depth is determined by about 10^{15} cm^{-3} shallow donors, the concentration of these deep traps with considering the λ-correction is ~4×10^{14} cm^{-3}. After irradiation, we detected the same center and a deeper electron trap at E_c-1 eV (electron capture cross section 4×10^{-13} cm^2). In C-V profiling of the space charge region, the entire 4.5 μm of the sample after irradiation was depleted of mobile carriers and the region probed in DLTS was much deeper than before irradiation [33-35]. Both types of deep traps detected previously in our κ-Ga_2O_3 films with thickness of 20 μm [26].

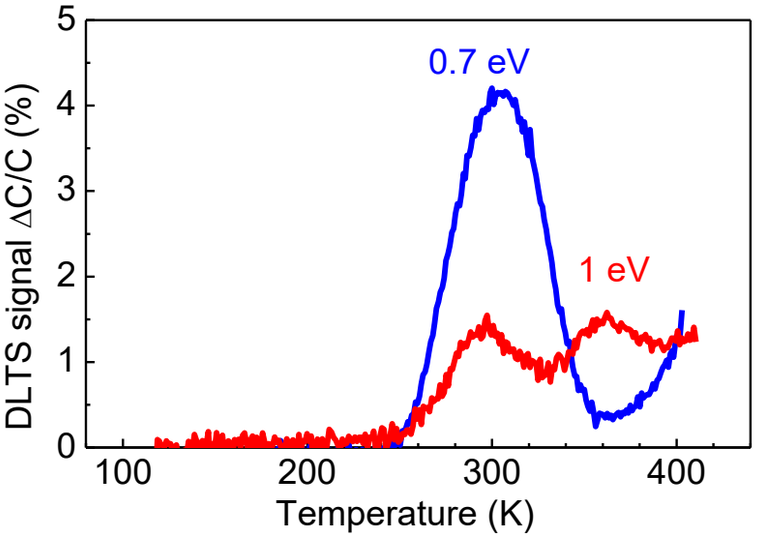

Fig. 4 (Color online) DLTS spectra measured at 10 kHz with reverse bias -1V, forward bias pulse of +1V (50 ms long), time window 0.4s/4s before (blue line) and after (red line) irradiation.

The dependencies of the EBIC current I_c normalized by the product of the SEM probing beam current I_b and beam energy E_b, $Ic/(I_b \times E_b)$, on the probing beam energy E_b are shown for the sample before and after irradiation in Fig. 5. The symbols represent experimental points, the solid lines are the results of fitting the observed dependence with diffusion length values of 70 nm and 80 nm, respectively, before and after irradiation [29]. The origin of the centers responsible for recombination of non-equilibrium charge carriers is not known now. We have not found reports of diffusion length measurements results in κ-Ga_2O_3. When compared to the values of diffusion lengths in lightly doped β-Ga_2O_3 films (200-800 nm in different samples [33]) the diffusion lengths in our κ-Ga_2O_3 are much shorter.

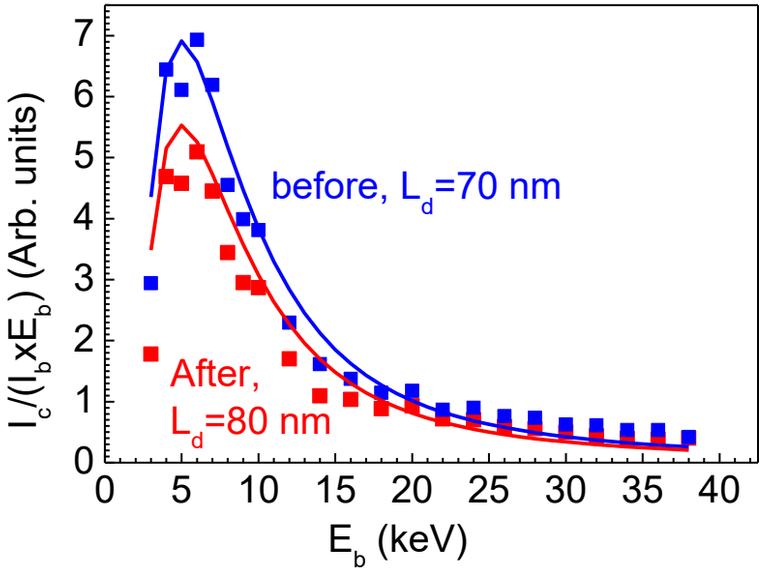

Fig. 5 (Color online) EBIC current normalized by the product of SEM probing beam current and energy before irradiation (solid blue squares) and after irradiation (solid red

squares); solid blue line is the result of fitting with diffusion length equal to 70 nm, solid red line is the result of fitting with diffusion length 80 nm.

IV. SUMMARY AND CONCLUSIONS

In summary, proton irradiation of thick κ-Ga_2O_3 sample with 1.1 MeV protons led to a strong decrease of centers providing charge carriers in the top 4.5 μm of the sample, so that the space charge region of the Schottky diode was fully depleted to this depth even at 0V bias. The width of this depleted region agrees with the projected range of 1.1 MeV protons from the Stopping and Range of Ions in Matter (SRIM) code [36]. This means all $2x10^{15}$ cm^{-3} deep and shallow donors in the upper 2.5 μm of the sample and 10^{15} cm^{-3} shallower donors with ionization energy 0.15 eV at deeper depths were removed by irradiation in the upper 4.5 μm. This leads to an electron removal rate by 1.1 MeV protons in n-type κ-Ga_2O_3 of ~ (10-20) cm^{-1}, close to the value for similarly lightly doped HVPE-grown α-Ga_2O_3 (carrier removal rate 35 cm^{-1}) [33-35] but is considerably lower than the carrier removal rate under similar conditions for lightly doped β-Ga_2O_3 where the effective removal rate was >100 cm^{-1} [33-35].

The origin of electron removal in κ-Ga_2O_3 by proton radiation is less clear than in the other polytypes. The density of deep acceptors estimated from LCV profiling is similar before and after irradiation and there are insufficient concentrations of deep electron traps to explain the carrier removal rates. The appearance of additional 1 eV electron traps after irradiation could be due to the change in the location from which the DLTS signal after irradiation was collected (~4.5 μm from the surface as opposed to ~2.5 μm from the surface before irradiation. In thinner κ-Ga_2O_3 films studied previously we observed both types of electron traps [26]. The diffusion length of non-equilibrium charge

carriers did not change after irradiation, in addition to the Micro cathodoluminescence (MCL) spectra [26] and intensity (Fig. S7 of the Supplementary Material). We propose the carrier removal in κ-Ga_2O_3 irradiated with protons is due to complexing of shallow donors with deep acceptors produced by protons, likely comprising Ga vacancies [35].

SUPPLEMENTAL MATERIAL

See supplementary material at [URL will be inserted by AIP Publishing] for additional characterization results from the samples.

ACKNOWLEDGMENTS

The work at NUST MISiS was supported in part by a grant from the Ministry of Science and Higher Education of Russian Federation (Agreement # 075-15-2022-1113). The work at UF was funded by the Defense Threat Reduction Agency (DTRA) as part of the Interaction of Ionizing Radiation with Matter University Research Alliance (IIRM-URA) under contract number HDTRA1-20-2-0002. The content of the information does not necessarily reflect the position or the policy of the federal government, and no official endorsement should be inferred. The work at UF was also supported by NSF DMR 1856662.

AUTHOR DECLARATIONS

Conflicts of Interest *(required)*

The authors have no conflicts to disclose.

DATA AVAILABILITY

The data that supports the findings of this study are available within the article and supplemental material.

REFERENCES

[1]S. J. Pearton, Fan Ren, Marko Tadjer, and Jihyun Kim, J. Appl. Phys. **124**, 220901 (2018).
[2] Gallium Oxide: Materials Properties, Crystal Growth, and Devices, ed. Masataka Higashiwaki and Shizuo Fujita (Springer Series in Materials Science ISBN 978-3-030-37152-4 ISBN 978-3-030-37153-1, 2020).
[3]S. Dahiya, Damanpreet Kaur, Anupam Ghosh and Mukesh Kumar, Materials Today Commun **33**, 104244 (2022).
[4] M.Bosi, P. Mazzolini, LSeavalli and R. Fornari, J.Mater. Chem C **8**, 10975 (2020).
[5]Kentaro Kaneko, Kazuyuki Uno, Riena Jinno, and Shizuo Fujita, J. Appl. Phys. **131**, 090902 (2022).
[6]J. Xu, W. Zheng and F. Huang, J. Mater. Chem. C, **7**, 8753 (2019).
[7]An-Chen Liu, Chi-Hsiang Hsieh, Catherine Langpoklakpam, Konthoujam James Singh, Wen-Chung Lee, Yi-Kai Hsiao, Ray-Hua Horng, Hao-Chung Kuo, and Chang-Ching Tu, ACS Omega **7**, 41, 36070 (2022).
[8]Andrew J. Green, James Speck, Grace Xing, Peter Moens, Fredrik Allerstam, Krister Gumaelius, Thomas Neyer, Andrea Arias-Purdue, Vivek Mehrotra, Akito Kuramata, Kohei Sasaki, Shinya Watanabe, Kimiyoshi Koshi, John Blevins, Oliver Bierwagen, Sriram Krishnamoorthy, Kevin Leedy, Aaron R. Arehart, Adam T. Neal, Shin Mou, Steven A. Ringel, Avinash Kumar, Ankit Sharma, Krishnendu Ghosh, Uttam Singisetti, Wenshen Li, Kelson Chabak, Kyle Liddy, Ahmad Islam, Siddharth Rajan, Samuel Graham, Sukwon Choi, Zhe Cheng, and Masataka Higashiwaki, APL Mater. **10**, 029201 (2022).
[9]Francesco Mezzadri, Gianluca Calestani, Francesco Boschi, Davide Delmonte, Matteo Bosi, and Roberto Fornari, Inorg. Chem. **55**, 12079 (2016).
[10]A. Parisini, A. Bosio, V. Montedoro, A. Gorreri, A. Lamperti, M. Bosi,G. Garulli, S. Vantaggio, and R. Fornari, APL Mater. **7**, 031114 (2019).
[11]H. von Wenckstern, Adv. Electron. Mater. **3**, 1600350 (2017).
[12]I. Cora, Zs. Fogarassy, R. Fornari, M. Bosi, A. Recnik, B. Pécz, Acta Mater **183**, 216 (2020).
[13]V. I. Nikolaev, S. I. Stepanov, A. I. Pechnikov, S.V. Shapenkov, M. P. Scheglov, A.V. Chikiryaka, and O. F. Vyvenko, ECS J. Solid State SC., **9**, 045014 (2020).
[14]V. Chikiryaka, S. I. Stepanov, O. S. Medvedev, S. V. Shapenkov, E. V. Ubyivovk and O. F. Vyvenko, J. Physics: Conf Ser, **1400**, 055049 (2019).
[15]M. Kracht, A. Karg, J. Schörmann, M. Weinhold, D. Zink, F. Michel, M. Rohnke, M. Schowalter, B. Gerken, A. Rosenauer, P. J. Klar, J. Janek, and M. Eickhoff, Phys. Rev. Appl. **8**, 054002 (2017).
[16]M. Kneiß, D. Splith, P. Schlupp, A. Hassa, H. von Wenckstern, M. Lorenz, and M. Grundmann, J. Appl. Phys. **130**, 084502 (2021).
[17]Anna Hassa, Charlotte Wouters, Max Kneiß, Daniel Splith, Chris Sturm,Holger von Wenckstern, Martin Albrecht, Michael Lorenz and Marius Grundmann, J. Phys. D: Appl. Phys. **53**, 485105(2020).
[18] S. Yusa, D. Oka, and T. Fukumura, CrystEngComm **22**, 381 (2020).

[19]M. Kneiß, P. Storm, A. Hassa, D. Splith, H. von Wenckstern, M. Lorenz, and M. Grundmann, APL Mater. **8**, 051112 (2020).
[20]J. P. McCandless, C. S. Chang, K. Nomoto, J. Casamento, V. Protasenko, P. Vogt, D. Rowe, K. Gann, S. T. Ho, W. Li, R. Jinno, Y. Cho, A. J. Green, K. D. Chabak, D. G. Schlom, M. O. Thompson, D. A. Muller, H. G. Xing, and D. Jena, Appl. Phys. Lett. **119**, 062102 (2021).
[21] Jin Wang, Hui Guo, Cheng-Zhang Zhu, Qing Cai, Guo-Feng Yang, Jun-Jun Xue, Dun-Jun Chen, Yi Tong, Bin Liu, Hai Lu, Rong Zhang, and You-Dou Zheng, IEEE Electr Device L. **41**, 1052, (2020).
[22] Sung Beom Cho and Rohan Mishra, Appl. Phys. Lett. **112**, 162101 (2018).
[23]A.Y. Polyakov, V.I. Nikolaev, A.I. Pechnikov, E.B. Yakimov, S. Yu. Karpov, S.I. Stepanov, I.V. Shchemerov, A.A. Vasilev, A.V. Chernykh, A. Kuznetsov, In-Hwan Lee, S.J. Pearton, J. Alloy Compd, **936**, 168315 (2023).
[24]Yuichi Oshima, Katsuaki Kawara, Takayoshi Oshima, and Takashi Shinohe, Jpn J. Appl. Phys. **59**, 115501 (2020).
[25]Hiroyuki Nishinaka, Osamu Ueda, Yusuke Ito, Noriaki Ikenaga, Noriyuki Hasuike, and Masahiro Yoshimoto, Jpn J. Appl Phys **61**, 018002 (2022).
[26]A.Y. Polyakov, V.I. Nikolaev, A.I. Pechnikov, S.I. Stepanov, E.B. Yakimov, M.P. Scheglov, I.V. Shchemerov, A.A. Vasilev, A.A. Kochkova, A.V. Chernykh, A.V. Chikiryaka, S.J. Pearton, APL Mater. **10**, 061102 (2022).
[27]S. I. Stepanov, V. I. Nikolaev, A. Y. Polyakov, A. I. Pechnikov, E. B. Yakimov, M. P. Scheglov, I. V. Shchemerov, A. A. Vasilev, A. A. Kochkova, A. V. Chernykh, A. V. Chikiryaka, P. N. Butenko, and S. J. Pearton, ECS J. Sol. State SC, **12**, 015002 (2023).
[28]Capacitance spectroscopy of semiconductors, ed. Jian V. Li and Giorgio Ferrari (Pan Stanford Publishing Pte Ltd, Singapore, 2018) 437 pp
[29] E. B. Yakimov, A. Y. Polyakov, N. B. Smirnov, I. V. Shchemerov, Jiancheng Yang, F. Ren, Gwangseok Yang, Jihyun Kim, S. J. Pearton. J. Appl. Phys. **123**, 185704 (2018).
[30]A. Y. Polyakov, N. B. Smirnov, I. V. Shchemerov, S. J. Pearton, F. Ren, A. V. Chernykh, P. B. Lagov, and T. V. Kulevoy, APL Mater. **6**, 096102 (2018).
[31]A. Y. Polyakov, N. B. Smirnov, I. V. Shchemerov, E. B. Yakimov, S. J. Pearton, Chaker Fares, Jiancheng Yang, Fan Ren, Jihyun Kim, P. B. Lagov, V. S. Stolbunov, and A. Kochkova, Appl. Phys. Lett. **113**, 092102 (2018).
[32] Z. Zhang, E. Farzana, A. R. Arehart, and S. A. Ringel, Appl. Phys. Lett. **108**, 052105 (2016).
[33]Alexander Y. Polyakov, Vladimir I. Nikolaev, Eugene B. Yakimov, Fan Ren, Stephen J. Pearton, and Jihyun Kim, J. Vac. Sci. Technol. A **40**, 020804 (2022).
[34]Xinyi Xia, Jian-Sian Li, Ribhu Sharma, Fan Ren, Md Abu Jafar Rasel, Sergei Pavlovich Stepanoff, Nahid Sultan Al-Mamun, Aman Haque, Douglas Wolfe, Sushrut Modak, Leonid Chernyak, Mark Law, Ani Khachatrian, Stephen J. Pearton, ECS J. Solid State SC. **11**,095001 (2022).
[35]Hemant J. Ghadi, Joe F. McGlone, Esmat Farzana, Aaron R. Arehart and Steven A. Ringel, Radiation Effects on β-Ga_2O_3 Materials and Devices, in Ultrawide Bandgap β-Ga_2O_3 Semiconductor: Theory and Applications, edited by James S. Speck and Esmat Farzana (AIP Publishing, Melville, New York, 2023), Chapter 12, pp. 12-1–12-26.
[36]J. F. Ziegler, M. D. Ziegler, and J. P. Biersack, Nucl. Instrum. Meth Phys. B **268**, 1818 (2010).

Journal of Vacuum Science & Technology A

PLEASE CITE THIS ARTICLE AS DOI: 10.1116/6.0002673

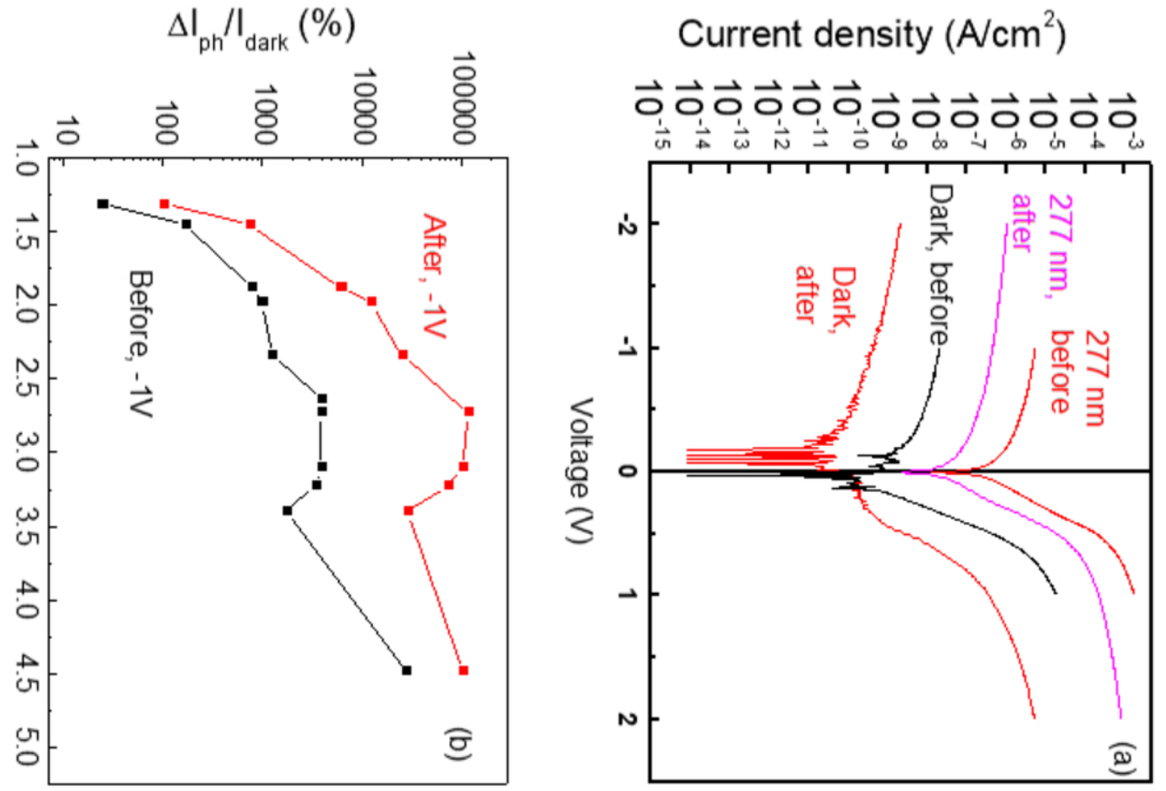

Journal of Vacuum Science & Technology A

PLEASE CITE THIS ARTICLE AS DOI: 10.1116/6.0002673

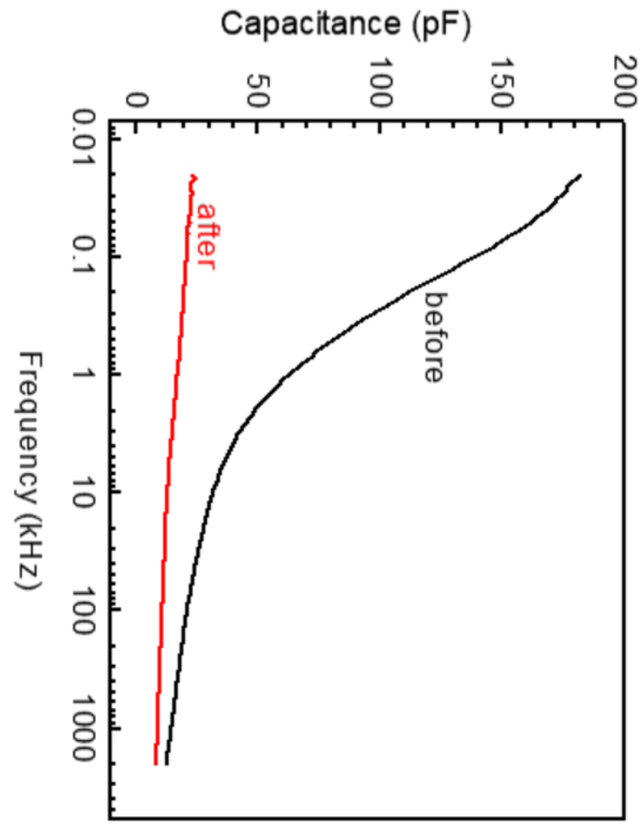

Journal of Vacuum Science & Technology A

PLEASE CITE THIS ARTICLE AS DOI: 10.1116/6.0002673

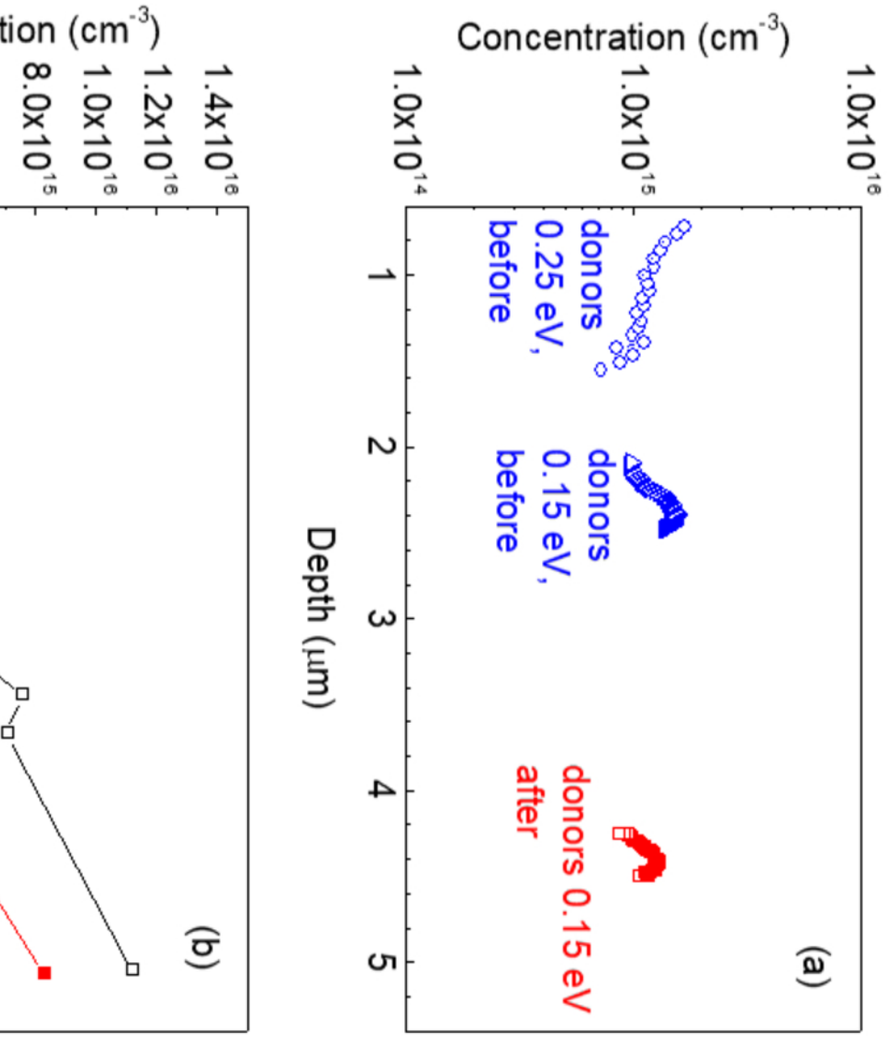

Journal of Vacuum Science & Technology A

PLEASE CITE THIS ARTICLE AS DOI: 10.1116/6.0002673

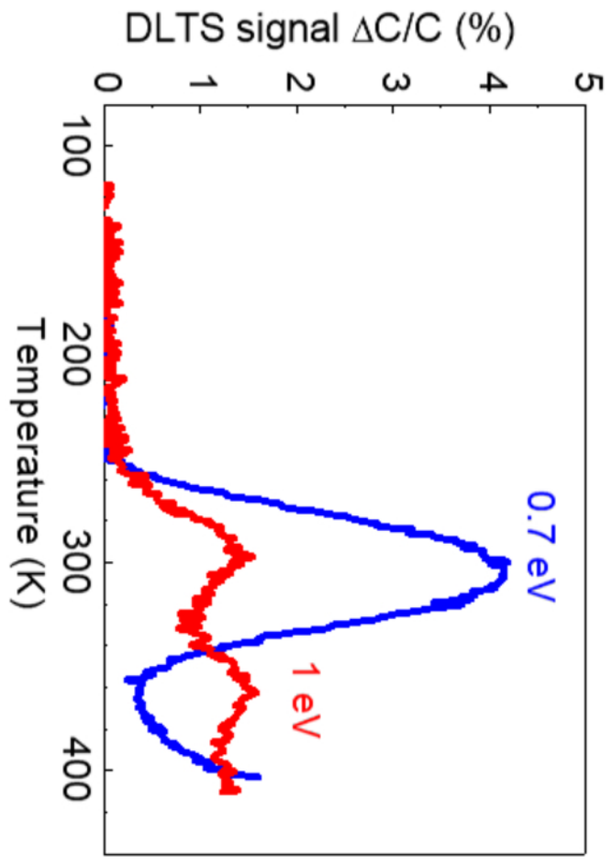

Journal of Vacuum Science & Technology A

PLEASE CITE THIS ARTICLE AS DOI: 10.1116/6.0002673